

Extracting spectral properties from Keldysh Green functions

Andreas Dirks,^{1,2} Martin Eckstein,³ Thomas Pruschke,¹ and Philipp Werner⁴

¹*Department of Physics, University of Göttingen, D-37077 Göttingen, Germany*

²*Department of Physics, Georgetown University, Washington, DC, 20057 USA*

³*Max Planck Research Department for Structural Dynamics,
University of Hamburg-CFEL, Hamburg, Germany*

⁴*Department of Physics, University of Fribourg, 1700 Fribourg, Switzerland*

(Dated: October 31, 2012)

We investigate the possibility to assist the numerically ill-posed calculation of spectral properties of interacting quantum systems in thermal equilibrium by extending the imaginary-time simulation to a finite Schwinger-Keldysh contour. The effect of this extension is tested within the standard Maximum Entropy approach to analytic continuation. We find that the inclusion of real-time data improves the resolution of structures at high energy, while the imaginary-time data are needed to correctly reproduce low-frequency features such as quasi-particle peaks. As a nonequilibrium application, we consider the calculation of time-dependent spectral functions from retarded Green function data on a finite time-interval, and compare the Maximum Entropy approach to direct Fourier transformation and a method based on Padé approximants.

PACS numbers: 02.70.-c, 71.15.Dx, 71.28.+d, 71.10.Fd, 64.60.Ht

I. INTRODUCTION

A common strategy to circumvent the oscillatory convergence of integrals in interacting quantum field theories is the Wick rotation to imaginary time. Apart from possible fermionic sign problems, quantum Monte Carlo (QMC) simulations are well-conditioned on the imaginary time axis, and simulations at non-zero temperature using the Matsubara technique are straightforward. However, extracting dynamic properties from imaginary-time data of the single-particle Green's function $G(-i\tau) = -\langle T_\tau c(\tau) c^\dagger(0) \rangle$ is an ill-posed problem: the singular integral equation

$$iG(-i\tau) = \int d\omega A(\omega) \frac{e^{-\tau\omega}}{1 + e^{-\beta\omega}} \quad (1)$$

has to be solved for the spectral function $A(\omega)$.

If the real-time data for the retarded Green's function

$$G^{\text{ret}}(t, t') = -i\Theta(t - t') \langle \{d(t), d^\dagger(t')\} \rangle \quad (2)$$

were known on the entire real-time axis, the spectral function could be obtained from a simple inverse Fourier transform (in equilibrium, $G^{\text{ret}}(t, t')$ depends only on the time difference $t - t'$). The Fourier transform is not ill-posed, due to unitarity. Unfortunately, calculating these real-time data for an interacting system is difficult. Monte Carlo techniques cannot reach long times, due to a dynamical sign problem which grows exponentially as a function of the maximum real time t_{max} . Nevertheless, as shown in Refs. [1–3] the real-time Green function up to some finite time t_{max} can be computed accurately using continuous-time Monte Carlo algorithms [4–7], or, in certain parameter regimes, using perturbative weak- [8] or strong-coupling methods [9, 10]. This raises the question if the information contained in the real-time correlators

for $t, t' < t_{\text{max}}$ can be exploited to obtain reliable spectra using a suitably adapted analytical continuation procedure.

A real need for the “analytical continuation” of real-time Green functions arises in the study of nonequilibrium properties of correlated systems, e. g. lattice systems perturbed by a quench or some field pulse [11–13]. In order to characterize the relaxation of these systems, it is often useful to define a time-dependent spectral function

$$A(\omega, t) = -\frac{1}{\pi} \text{Im} \int_t^\infty dt' e^{i\omega(t'-t)} G^{\text{ret}}(t', t), \quad (3)$$

where $G^{\text{ret}}(t', t)$ now depends on both times individually due to the loss of time-translation invariance. $A(\omega, t)$ is not assured to be positive, but it typically becomes positive a short time after the perturbation. (In particular, $A(\omega, t)$ is positive for any quasi-stationary state. When $A(\omega, t)$ is constant over a time window of width Δt , then $A(\omega, t)$ must be positive after averaging over a frequency window of $\Delta\omega \propto 1/\Delta t$.) Under certain assumptions, $A(\omega, t)$ is related to the photoemission and inverse photoemission signal [14, 15]. Furthermore, in an equilibrium system, Eq. (3) reduces to the familiar spectral function defined in Eq. (1). The challenges in the evaluation of $A(\omega, t)$ are the same as those for equilibrium spectra mentioned above: In practice, simulation results will be limited in time, so direct Fourier transformation will lead to oscillations or a smearing-out of spectral features. Therefore, a second question which we want to address is whether Maximum Entropy or Padé approaches can be used to improve the quality of these time-dependent spectra.

The paper is structured as follows: in Sec. II we present and test the Maximum Entropy approach for Keldysh Green's functions. In particular, Sec. II B investigates the singular values of the kernel matrix and their depen-

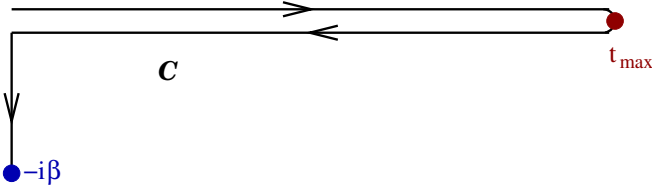


FIG. 1: (color online) The Schwinger-Keldysh contour \mathcal{C} . Arrows denote the direction of time-ordering $<_{\mathcal{C}}$.

dence on the choice of data points, in Sec. II C we test the analytical continuation procedure for exactly known Green's functions, and in Sec. II D we compare the Maximum Entropy result to spectra obtained by Fourier transformation. A generalization of the Padé analytical continuation procedure to nonequilibrium Green functions is introduced in Sec. III. In Sec. IV we apply the Maximum Entropy method to real-time simulation data of equilibrium and nonequilibrium systems, and compare the method to direct Fourier transformation and the Padé procedure. Sec. V gives a summary and conclusion.

II. MAXIMUM ENTROPY APPROACH

A. Formulation of the problem

In practice, real-time simulations are carried out on the Keldysh contour \mathcal{C} [16, 17] illustrated in Fig. 1. The Green's function is a function of two time indices t and t' , which may lie on the upper real, the lower real, or the Matsubara branch of the contour. Using the Keldysh-contour time-ordering $<_{\mathcal{C}}$, the contour-ordered equilibrium Green's function is related to the spectral function through

$$\begin{aligned} iG(z, z') &= \langle T_{\mathcal{C}} d(z) d^{\dagger}(z') \rangle \\ &= \int d\omega A(\omega) e^{-i(z-z')\omega} F_{z, z'}(\omega), \end{aligned} \quad (4)$$

with the contour-ordered Fermi factor

$$F_{z, z'}(\omega) := \begin{cases} f(-\omega) & \text{if } z' <_{\mathcal{C}} z, \\ -f(\omega) & \text{else,} \end{cases} \quad (5)$$

and the times z, z' located on \mathcal{C} . Obviously, Eq. (4) is a generalization of Eq. (1), and extracting $A(\omega)$ from any data set $G(z_i, z_j)$ is still an ill-posed problem when the times z_i are restricted to the Matsubara branch, or to times smaller than some finite t_{\max} .

The Maximum Entropy analytic continuation procedure involves the inference of a *most probable* spectral function $A(\omega)$ among those which are compatible with the simulated data. The problem can be expressed in the matrix form

$$D = K \cdot A, \quad (6)$$

where D represents simulation data, K is a linear operator, given by the matrix kernel, applied to the unknown spectral function A . The finite set D can be interpreted as a snapshot from a Gaussian random variable with covariance C , in the case of a Monte Carlo simulation [19].

The essential idea for inferring a most probable A from D has been outlined in Ref. [19]. An entropy functional $\alpha S[A]$ is added in order to regularize the minimization of $\chi^2[D, A]$ with respect to A , where

$$\chi^2[D, A] := \frac{1}{2} (KA - D)^T C^{-1} (KA - D). \quad (7)$$

The most informative scalar α can be determined by a systematic application of Bayesian inference (*Classic MaxEnt*), or can be averaged over the corresponding Bayesian probability distribution (*Bryan's MaxEnt*).

The standard numerical algorithm for the maximum entropy inference of spectral functions was developed by Bryan [21]. The kernel is decomposed via a singular-value decomposition

$$K = V \Sigma U^T, \quad (8)$$

where $\Sigma = \text{diag}(\sigma_1, \sigma_2, \dots)$, $\sigma_1 \geq \sigma_2 \geq \dots \geq 0$. Through the matrix products, each singular value σ_i is associated with a direction in A -space and a direction in D -space. The former is given by one of the “basis functions” for the spectral function and the latter is represented by an entry of V .

If σ_i is large, it provides a channel which transports a comparably large amount of information about A . If σ_i is small, not much information can be gained for the corresponding direction in A -space, and the Bayesian approach will not modify a default spectrum with respect to that direction, due to a lack of evidence. A small value of σ can only be compensated by small error bars for the corresponding D -direction. Hence, the shape of the singular value distribution is an important indicator for the structure of the inverse problem.

B. Singular value distributions

In this section we analyze the singular value structure of the integral kernel K in Eq. (6), for various data sets D (the set A is always given by some appropriate discretization of the spectral function). In panel (a) of Fig. 2 the singular value distribution is plotted for the usual inference from imaginary-time data (solid lines), for inverse temperature $\beta = 10$. In this case, the data set $D = D_{\text{imag}}$ consists of the values $G(-i\tau_j, 0)$ on N equidistant points on the imaginary time branch,

$$D_{\text{imag}}^{N, \beta} = \{G(-i\tau_j, 0) \mid \tau_j = \beta j/N, j = 0, \dots, N-1\}. \quad (9)$$

The singular values are seen to decay exponentially.

Next we define a suitable data set for extracting $A(\omega)$ from pure real-time data. We note that the imaginary-time set of input data contains real-time information for

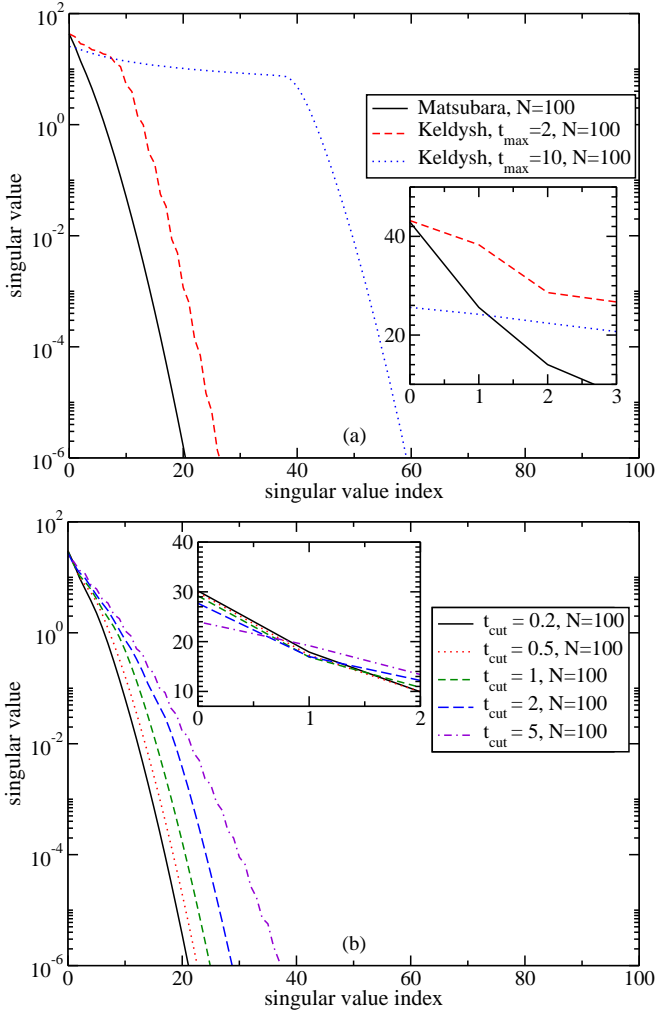


FIG. 2: (color online) Singular value distributions for $\beta = 10$ and indicated number of time-points N . Panel (a): Matsubara and real-time Green's functions. Panel (b): Keldysh-offdiagonal Green's functions.

both positive (forward direction) and negative (backward direction) frequencies. In the case of real-time data, the situation is different: If only one time ordering of d, d^\dagger is taken into account, the Maximum Entropy method only yields information about the positive or negative frequency range, i. e. the occupied and unoccupied part of the spectrum. It is thus important to consider “lesser” and “greater” (or retarded) Green's functions. We choose (z, z') values that correspond to both electrons propagating forward in time starting from $t' = 0$, $G^>(t, 0) = -i\langle d(t)d^\dagger(0) \rangle$, and backward in time starting from $t' = t_{\max}$ along the upper real-time branch, $G^<(t, t_{\max}) = i\langle d^\dagger(t_{\max})d(t) \rangle$, using an equidistant grid of annihilation times,

$$D_{\text{real}}^{N, t_{\max}} = \{\text{Re}G^>(t_j, 0), \text{Im}G^>(t_j, 0), \text{Re}G^<(t_j, t_{\max}), \text{Im}G^<(t_j, t_{\max}) \mid t_j = jt_{\max}4/N, j = 0, \dots, N/4 - 1\}. \quad (10)$$

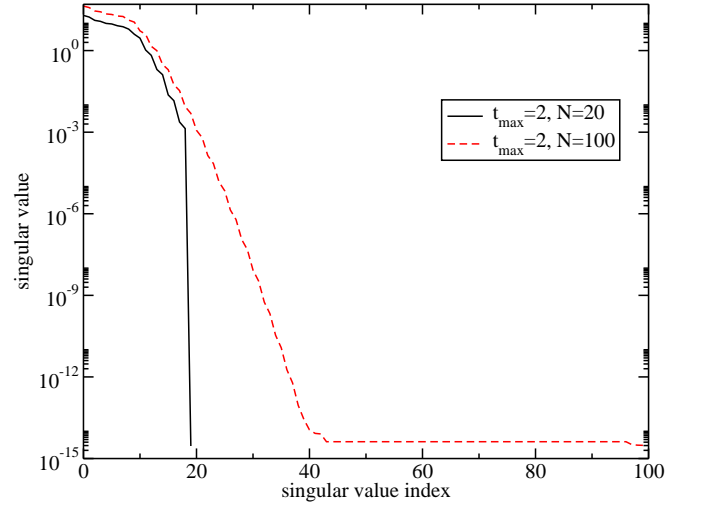


FIG. 3: (color online) Dependence of real-time singular value distributions on the number of input data N in $D_{\text{real}}^{N, t_{\max}}$.

Due to translational invariance, the d^\dagger operator need not be shifted in time. Since we use both the real and imaginary parts of $G^>(t, 0)$ and $G^<(t, t_{\max})$ each time step contributes two real variables to the inference process, and we always use N for the the total number of real variables below.

In contrast to the case of imaginary-time input, the kernel for pure real-time propagators has a distinguished plateau in its singular value distribution, even for rather small $t_{\max} = 2$ (dashed line in Fig. 2). As t_{\max} is increased ($t_{\max} = 10$, dotted line), the plateau broadens, and more equally dominant A -directions appear. This is because in the limit $t_{\max} \rightarrow \infty$ the (no longer ill-posed) unitary limit $\sigma_i \equiv 1$ is approached.

We next consider singular-value distributions for Keldysh-offdiagonal propagators. For symmetry reasons we can restrict ourselves to mixed Green functions from the upper Keldysh contour to the imaginary branch, $G^\Gamma(\tau, t_{\text{cut}})$. We consider fixed values of t_{cut} . $t_{\text{cut}} = 0$ is equivalent to the usual kernel for the Matsubara Green's function. As t_{cut} is increased, the singular value distribution is broadened (panel (b) of Fig. 2), but not as dramatically as in panel (a) of Fig. 2. Keeping $\tau = \tau_{\text{cut}}$ fixed yields a structure more similar to the real-time distributions in panel (a) ($\tau_{\text{cut}} = 0$ is exactly the same). However, it appears that the plateaus in panel (a) cannot be exceeded.

Figure 3 shows the dependence of the real-time singular-value distribution on the number N of time-points, for a Keldysh contour length $t_{\max} = 2$. We find that at low singular value indices, apart from a finite offset, the same shape is obtained. In particular, the same number of singular values is associated with the plateau. Furthermore, the initial descent from the plateau is also identical. However, the singular value distribution for $N = 100$ continues to decrease smoothly, whereas the corresponding curve for $N = 20$ abruptly

jumps to the lowest singular value which is of the order of 10^{-15} . A similar behaviour is also found for other correlators within the Keldysh contour.

We conclude that increasing N does not extend the width of the plateau (once the latter has been established), but merely adds further singular values to the rapidly decreasing tail. Since this decrease is exponential, an increase in N is only useful if the added singular values are larger than the order of magnitude ε of the numerical error of the data. This dependence is indeed observed in the data analysis presented in the following subsections.

C. Tests of equilibrium spectral functions

We will first analyze the behaviour of the continuation procedure using artificial data sets corresponding to given spectral functions with sharp peaks or band edges. For this purpose, uncorrelated data sets taken from the exact contour Green function are studied, and we assume a uniform error distribution ε , i.e., the covariance matrix is taken to be of the form $C = \text{diag}(\varepsilon^2)$. The performance of the Maximum Entropy procedures on more realistic data sets will be investigated in Sec. IV.

1. Rectangular spectrum

As a first test case we consider the rectangular spectral function

$$A_{\text{rect}}(\omega) := \frac{1}{4} \cdot \begin{cases} 1, & \text{if } |\omega| < 2, \\ 0, & \text{else.} \end{cases} \quad (11)$$

It can be expected that the sharp band edges will be difficult to infer from any finite data set. It is well-known that even the inverse Fourier transform, i.e. the unitary limit $t_{\text{max}} \rightarrow \infty$ converges only slowly, and that the convergence is not point-wise. Hence, we consider this an interesting test case for the Maximum Entropy method. The analytic continuation procedure is tested for inverse temperature $\beta = 10$ and for real-branch lengths $t_{\text{max}} = 2$ and $t_{\text{max}} = 10$. The fake variance of all \mathcal{C} -contour correlator estimators is set to $\varepsilon^2 = 6 \cdot 10^{-14}$.

Figure 4 compares the exact spectral function to the $A(\omega)$ obtained from the analytical continuation for different data sets (9) and (10). The total number of real variables is kept constant at $N = 100$, i.e., we use either 100 equidistant time steps on the imaginary axis, or 25 time steps in the real-time set $D_{\text{real}}^{N, t_{\text{max}}}$. (We found that the restriction of real input data to the real or imaginary parts of $G(t, t')$ does not contain sufficient information for an analytical continuation.)

In Fig. 4 it can be seen that using a broad Gaussian default model, the width of which has no significant influence on the results, the maximum entropy solution shows Gibbs ringing artifacts. The frequency of these

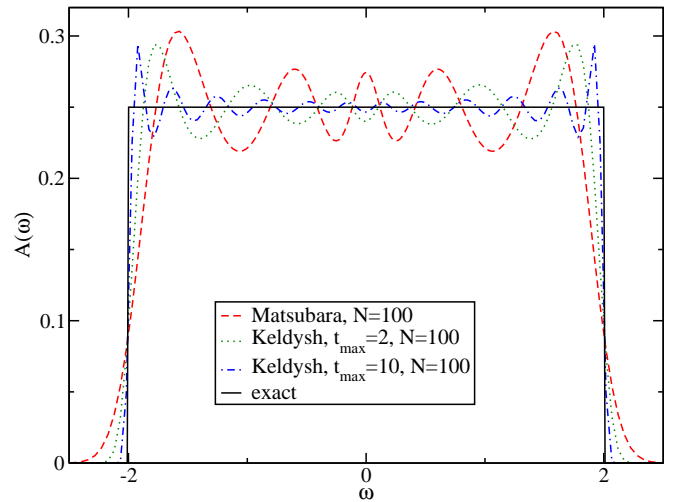


FIG. 4: (color online) Comparison of spectra at $\beta = 10$ for $N = 100$ data points located on the Matsubara contour, or on the upper Keldysh contour up to time $t_{\text{max}} = 2, 10$.

oscillations is a measure of the accuracy of the inferred spectrum. Surprisingly, already the real-time data from a short Keldysh branch, $t_{\text{max}} = 2$, yield more accurate results than the $\beta = 10$ Matsubara branch data. As t_{max} is increased, the approximation of the spectrum becomes even better.

Further increasing the number of data points N does not significantly change the above results. However, lowering the variance ε^2 and then raising N systematically yields more accurate spectra for both, Matsubara and Keldysh data, because in this case the requirements for the identity theorem of complex analysis which guarantees uniqueness are approached systematically. However, the convergence is always exponentially slow, as pointed out in the discussion of the dependence of the singular-value distributions on N .

2. Asymmetric triangle

We next investigate

$$A_{\text{triag}}(\omega) := \frac{1}{2} \cdot \begin{cases} \omega - 1, & \text{if } |\omega - 2| < 1, \\ 0, & \text{else} \end{cases} \quad (12)$$

as an example for spectra which are not particle-hole symmetric and for which the convergence of the inverse Fourier transform is more rapid than for the rectangular case. The variance is again set to $\varepsilon^2 = 6 \cdot 10^{-14}$. Results for this scenario are shown in Fig. 5. Judged by the peak position and the steepness at the discontinuity, even the $t_{\text{max}} = 0.2$ Keldysh spectrum is already slightly better than the Matsubara spectrum. This indicates that real-time data are good for resolving *high-energy features*,

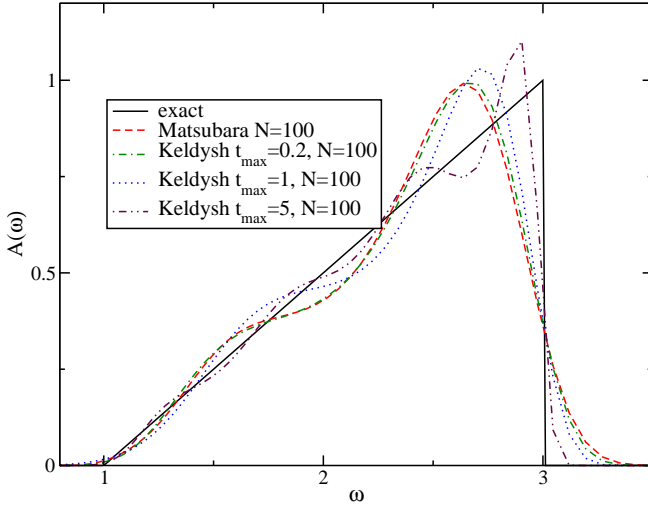


FIG. 5: (color online) Comparison for the triangular spectrum.

since the triangle is shifted to relatively high energies. As in the case of the rectangular shape, the spectrum improves as t_{\max} is increased.

3. Multiple peaks

As a next step towards more realistic situations we turn to a spectrum with a sharp resonance at $\omega = 0$ and two side bands. We model this by superimposing Gaussians,

$$A_{\text{peak}}(\omega) := \sum_{\alpha=\pm 1} c_{\text{sb}} g_{\sigma_{\text{sb}}, \alpha \Omega}(\omega) + c_{\text{res}} g_{\sigma_{\text{res}}, 0}(\omega), \quad (13)$$

with $c_{\text{res}} = 0.1$, $c_{\text{sb}} = 0.45$, $\Omega = 2.0$, $\sigma_{\text{sb}} = 0.5$, $\sigma_{\text{res}} = 0.05$; $g_{\sigma, X}(x) := \frac{1}{\sqrt{2\pi}\sigma^2} \exp\left(-\frac{(x-X)^2}{2\sigma^2}\right)$.

As one can see in Fig. 6, real-time data on relatively short contours ($t_{\max} = 2, 10$) are not particularly useful, when sharp *low-frequency* features such as the given “quasi-particle peak” should be extracted. The Matsubara data and the short- t_{\max} real-time data yield side bands of similar quality, while the imaginary-time data produce a comparable or even better reconstruction of the sharp resonance. Increasing t_{\max} mainly improves the resolution of smooth high-energy features ($t_{\max} = 10$, $N = 400$). We also observe that using $n = N/4 = 5$ equidistant time steps on the $t_{\max} = 2$ real contour yields a better spectrum than a similar data set on the $t_{\max} = 10$ contour. This finding is compatible with the earlier suggestion that as a function of N , a full establishment of the singular value plateau is crucial. However, increasing N at fixed t_{\max} involves only a polynomial increase of the computational effort, so we can always assume that N is sufficiently large for the plateau to be fully developed.

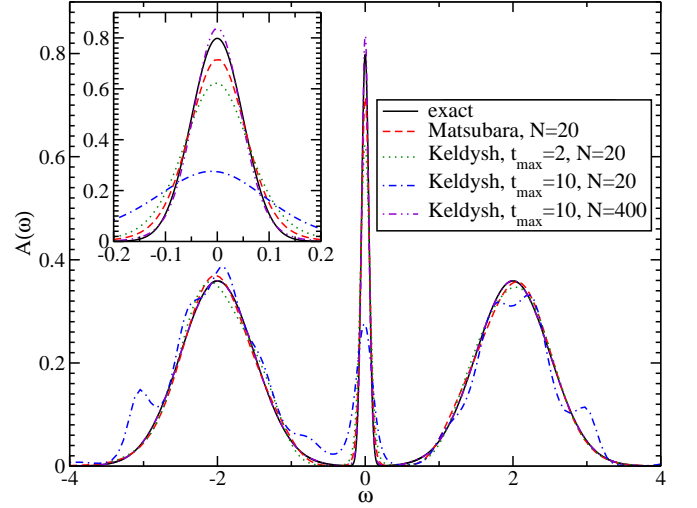


FIG. 6: (color online) Comparison for the three-peak spectrum.

Considering a broader selection of points from $G^{\Gamma}(\tau, t)$ data, we did not find an improvement of quality of the spectral function compared to pure Keldysh Green’s functions.

D. Comparison to direct inversion

The maximum entropy deconvolution is superior to direct inversion of the Fourier transform for finite Keldysh branches. To demonstrate this, we apply the usual rotation in Keldysh space and consider the retarded Green’s function defined in Eq. (2). In contrast to Eq. (4), no Fermi factor appears in the transform from the spectral function here,

$$iG^{\text{ret}}(t - t') = \int_{-\infty}^{\infty} d\omega e^{-i\omega(t-t')} A(\omega), \quad t > t'. \quad (14)$$

In the limit of a Keldysh contour of infinite length, a Laplace transform restores the spectral function

$$A(\omega) = -\text{Im} \frac{1}{\pi} \int_0^{\infty} dt e^{+i\omega t} G^{\text{ret}}(t). \quad (15)$$

For our contour of finite length t_{\max} a straightforward approximation to the deconvolution problem involves a truncation of the Laplace integral at time t_{\max} . Figure 7 shows spectra resulting from this method for the rectangular test spectrum and contour lengths $t_{\max} = 2$ and $t_{\max} = 10$.

Comparison to the finite- ε maximum entropy results from Keldysh propagators in Fig. 4 shows that the sharp edge is not resolved as well. Furthermore, unphysical regions of negative spectral weight appear in the case of the truncated Laplace transform, whereas this is avoided by construction in the maximum entropy approach. The

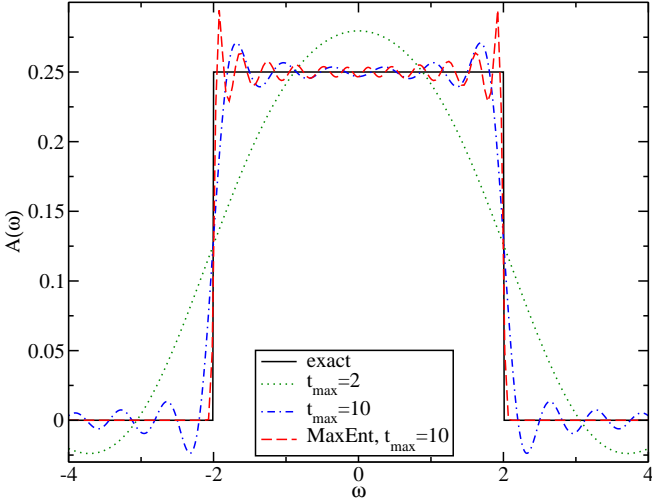


FIG. 7: (color online) Spectra obtained from retarded Green's function on the Keldysh contour using a truncated Laplace transform ($t_{\max} = 2$ and $t_{\max} = 10$) and comparison to the exact result. The $t_{\max} = 10$ Maximum Entropy result is included for comparison. See Fig. 4 for a more detailed comparison with Maximum Entropy data.

amplitude of the ringing oscillations seems to be almost the same as in the maximum entropy case, except near the band-edge, where the truncation involves an arbitrary smoothening of sharp structures. Different cut-off procedures for the time integral would yield different smoothenings of the spectrum.

III. PADÉ APPROXIMATION

As a second alternative to the Maximum Entropy approach, we consider the Padé method, which in equilibrium situations is often superior to the Maximum Entropy method for the analytic continuation of data without, or with very little stochastic noise. In particular for the analytical continuation of low-temperature Matsubara data, it is known to be rather precise at low frequencies [24].

The Padé approximant is constructed as follows: We assume that the values of the Green's function are known on a set of N points z_n in the complex frequency plane. Conventionally, the z_n are given by the Matsubara frequencies $i\omega_n$ ($\omega_n = (2n+1)\pi/\beta$). The Green function is interpolated with a rational function $C_N(z)$ in the form of a continued fraction,

$$C_N(z) = \frac{a_1}{1+} \frac{a_2(z-z_1)}{1+} \dots \frac{a_N(z-z_{N-1})}{1}, \quad (16)$$

where the coefficients a_i of the continued fraction are computed using a simple recursion formula [25].

In the present paper we are in particular interested in the non-equilibrium situation, i.e. the determination of a time-dependent spectral function $A(t, \omega)$ from the

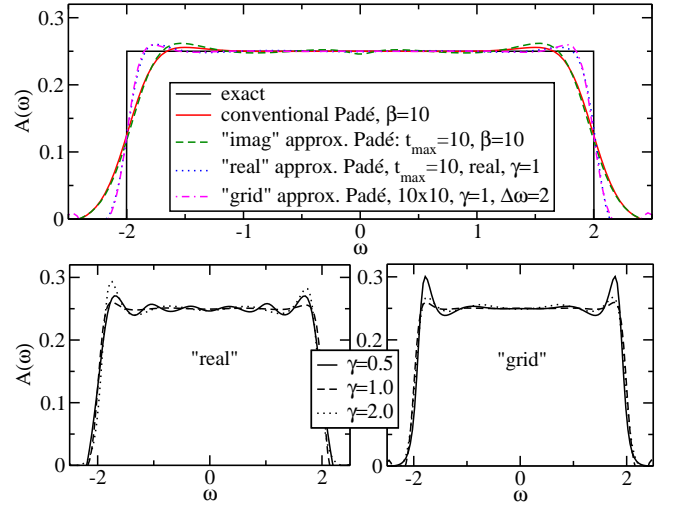


FIG. 8: (color online) Approximation of the rectangular spectrum with the Padé approach, either exact or for $t_{\max} = 10$. See Figs. 4 and 7 for comparison with Maximum Entropy and the truncated Laplace transform.

real-time retarded Green's function on some finite time interval $[t, t + \Delta t]$. For a set of points z_n in the complex plane, we first compute an approximation $\tilde{G}(t, z_n)$ of the Fourier transformed G^{ret} ,

$$\tilde{G}(t, z_n) := \int_t^{t+\Delta t} G^{\text{ret}}(t', t) e^{iz_n(t'-t)} dt'. \quad (17)$$

This approximation is good if the imaginary part of z_n is sufficiently large ($\text{Im } z_n \gg 1/\Delta t$). One can then construct a Padé approximant to the function $\tilde{G}(t, z)$ which tends to suppress the artificial oscillatory behaviour of spectral functions obtained from direct Fourier transforms (corresponding to $z \rightarrow \omega + i0^+$).

For the approximate Padé method we consider the following three variants: the points z_n are

- “imag”: fermionic Matsubara frequencies $z_n = i\omega_n = i(2n+1)\pi/\beta$, with some arbitrarily chosen β ,
- “real”: real frequencies with some imaginary offset $i\gamma$, i.e. $z_n = n\Delta\omega + i\gamma$,
- “grid”: arranged on a $N_{\text{real}} \times N_{\text{imag}}$ grid, where $z_{n_{\text{real}}n_{\text{imag}}} = \omega_{n_{\text{real}}}^{(r)} + i\omega_{n_{\text{imag}}}^{(i)}$. The lattice is chosen to be equidistant, with $\omega_{n_{\text{real}}}^{(r)} - \omega_{n_{\text{real}}-1}^{(r)} = \Delta\omega$ and $\omega_{n_{\text{imag}}}^{(i)} - \omega_{n_{\text{imag}}-1}^{(i)} = \omega_1^{(i)} =: \gamma$.

Figure 8 shows spectra obtained from these different Padé variants, when applied to the rectangular test spectrum. For the approximate Padé versions we always use the Keldysh contour length $t_{\max} = 10$, as well as 100 data points as input for any of the Padé procedures. It is interesting to note that, as compared to the truncated Laplace transform and the Maximum Entropy approach, the amplitude of the oscillations is significantly smaller

for the conventional Padé. However, the resolution of the jump is clearly limited. As β is decreased for the Matsubara frequencies, a slight increase of the slope can be observed.

Let us now discuss the approximate Padé method for a time interval length $t_{\max} = 10$. By construction it is closely related to the truncated Laplace transform, whose results are shown in Fig. 7. Nevertheless, features of the original Padé approach are also inherited, depending on how the z_n are chosen. In fact, the “imag” solution is much closer to the conventional Padé solution than to the respective truncated Laplace transform. The undesirable oscillations have been smoothened at the price of a reduced resolution at higher frequencies, while some of the oscillations from the truncated Laplace transform survive. For $\gamma = 1$, the “real” and “grid” solutions are almost identical. These results are closer to the exact solution than the truncated Laplace transform, even near the jump, and also exhibit smaller amplitude oscillations. Unfortunately, as shown in the lower panels, the rather unsystematic behaviour as a function of γ makes it difficult to determine the optimal value of γ a priori. We also note that in the “real” variant, the truncated Laplace solution is recovered for $\gamma = 0.5$, since in this case all the z_n are close to the real axis.

IV. APPLICATION TO DYNAMICAL MEAN FIELD RESULTS

A. Equilibrium spectra

As a realistic application, we analyze data obtained for the Kondo lattice model (bandwidth 4, $\beta = 50$, $J = 1.5$, 3.0) within dynamical mean field theory in Ref. [26], using the non-crossing approximation (NCA) as impurity solver. We do not want to discuss here the physics of the Kondo lattice model, and to what extent certain high energy features in the spectral function may be an artifact of the NCA. We merely use the results of Ref. [26] as a nontrivial example involving low-energy quasi-particle peaks and high-energy satellites.

In order to apply the Maximum Entropy Method (MEM), we again assume a uniform error ε and set off-diagonal entries of the covariance to zero. This seems justified as long as the systematic numerical error of the simulation data is significantly smaller than ε . In practice, the value of ε can be rather easily determined by trial and error: if ε is chosen too small, the MEM ceases to converge, whereas if it is chosen too large, the data lack sufficient information. In the following calculations, ε is chosen slightly larger than the value at which the MEM breaks down. This moves the systematic numerical errors just into the ε -range of the Gaussian statistical errors which are formally assumed by the Maximum Entropy procedure. As input data we consider the Matsubara Green’s functions $G^M(\tau)$ and the retarded (equilibrium) Green’s functions $G^{\text{ret}}(t - t')$, as well as data sets con-

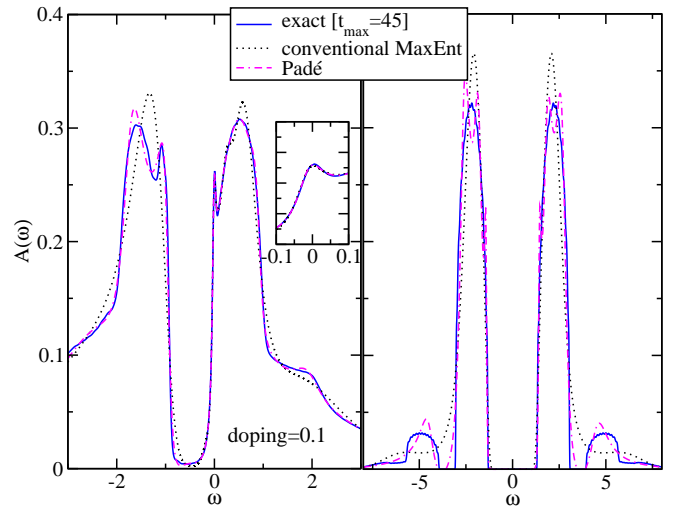


FIG. 9: (color online) Comparison of Padé and conventional MEM spectra for a Kondo lattice model (bandwidth 4, inverse temperature $\beta = 50$), in the Fermi-liquid regime ($J = 1.5$, left) and Kondo insulating regime ($J = 3.0$, right).

taining information from both Matsubara and retarded Green’s functions.

The NCA data considered here are noise-free low temperature data, and thus ideally suited for the Padé method. In Fig. 9 we compare MEM, Padé, and exact spectra for a half-filled Kondo-insulator, and a doped heavy-Fermi liquid solution. The “exact” spectra have been obtained from a truncated Laplace transformation with large $t_{\max} \approx 45$. We see that both Padé and Matsubara MEM reproduce the low-energy features and the gap-edges very well, but the higher energy structures cannot be accurately resolved.

In Fig. 10 we show in addition to the exact and Matsubara MEM spectra the results from a MEM analytical continuation of real-time data with $t_{\max} = 10$ and of a MEM continuation involving both the real-time and the imaginary-time data. The real-time MEM spectra produce the correct high-frequency behavior, and at least qualitatively correct structures in the lower band of the doped system, but they fail to reproduce the quasi-particle peaks. By adding also the imaginary-time data, we can accurately resolve the low-energy behavior (see insets), in addition to the high-energy structures. The main challenge in the equilibrium case thus remains the calculation of spectral features in the intermediate-energy range, where the convergence to the exact result with increasing t_{\max} is relatively slow.

B. Time-dependent spectra

To test the ability of the MEM approach to extract time-dependent spectra, we again consider results from Ref. 26. These spectra correspond to a perturbed, doped Kondo-lattice model which dissipates energy to a heat-

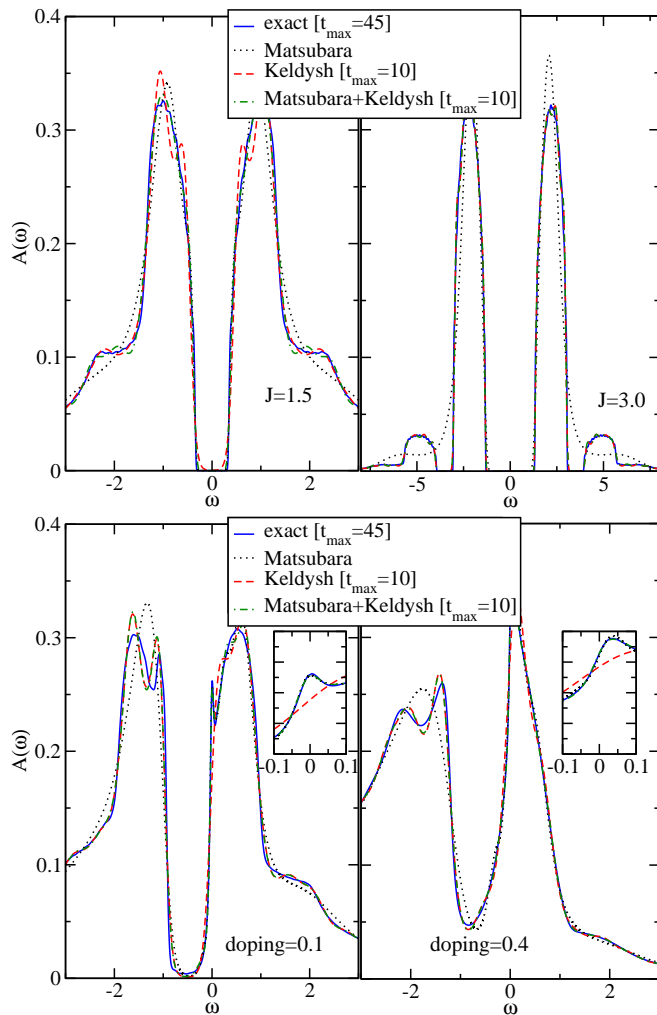


FIG. 10: (color online) Comparison of MEM solutions for the insulating Kondo lattice model (top, $J = 1.5$ and 3.0) and the doped heavy Fermi liquid regime (bottom, $J = 1.5$). A real-time contour length $t_{\max} = 10$ is sufficient to extract the relevant features.

bath, and thereby evolves from the high-temperature local moment regime into the low-temperature heavy-Fermi liquid regime. Again, we are not interested in the physics here, which has been discussed in Ref. [26], but just in the quality of the spectral functions that can be extracted from the retarded Green functions. In particular, we want to investigate the constraints on t_{\max} for the extraction of a time-dependent spectral function at time t ($t < t_{\max}$), since most computational techniques are limited to short time contours.

The upper panels of Fig. 11 show the spectral function $A(\omega, t)$ at a relatively short time $t = 6$ after the perturbation. As can be seen, $A(\omega, t)$ is already positive over the whole relevant frequency range. The different curves in the figure correspond to different time windows $[t, t + \Delta t]$ used in the MEM analytical continuation. The result for the largest Δt (dash-dotted curve) can be considered the exact result. We learn from these results that

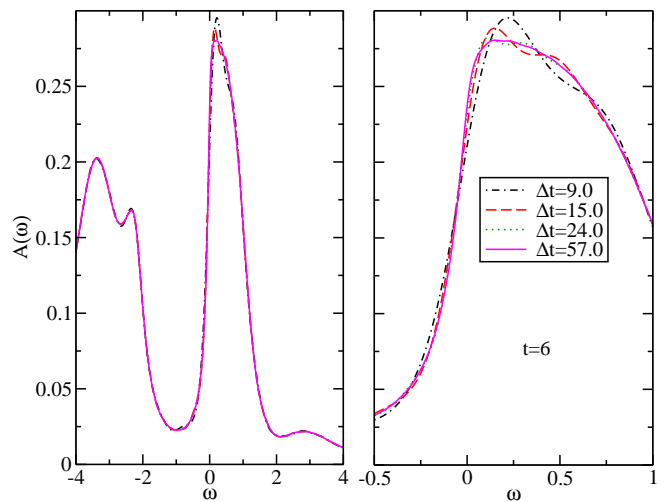


FIG. 11: (color online) Convergence of $A(\omega, t = 6)$ for different time-intervals $[t, t + \Delta t]$.

the high-frequency part converges very quickly with Δt , while we need at least an interval of length $\Delta t = 24$ to get a reasonably accurate result at low energies. (Since this calculation is a real nonequilibrium application, we cannot resort to Matsubara data to fix the low-energy part of the spectral function.)

A relevant question is how the MEM approach performs compared to direct Fourier transformation on an identical time interval. While both the MEM method and the direct Fourier transformation have difficulties reproducing the correct low-energy peak, the MEM spectra are slightly closer to the correct result.

C. Convergence of high-energy features

While the convergence of the MEM result for pure real-time Green's function data as a function of Δt is slow for the quasi-particle peak, it is interesting to see how the higher-energy features of the non-equilibrium spectral function converge to the exact result.

Figure 12 shows a comparison of the MEM result to the direct Fourier transform and the modified Padé method (discussed in Sec. III) for short time intervals with lengths $\Delta t \in [3.9, 5.7]$. For $\Delta t = 5.7$, MEM and direct Fourier transformation produce the correct solution, except in the low-energy region $-0.5 \lesssim \omega \lesssim 0.5$, the modified Padé method for the imaginary time interval yields spurious results. For shorter interval lengths, the MEM appears to be slightly superior to both, direct Fourier transform and modified Padé. All qualitative features of the spectrum, including the double-peak structure in the lower band start to become visible in the MEM solution at $\Delta t = 4.5$, whereas the emergence of similar structures in the direct FT spectrum at $\Delta t = 5.1$ may still be interpreted as part of the overall oscillatory behaviour of that solution. One may thus argue that the MEM reduces

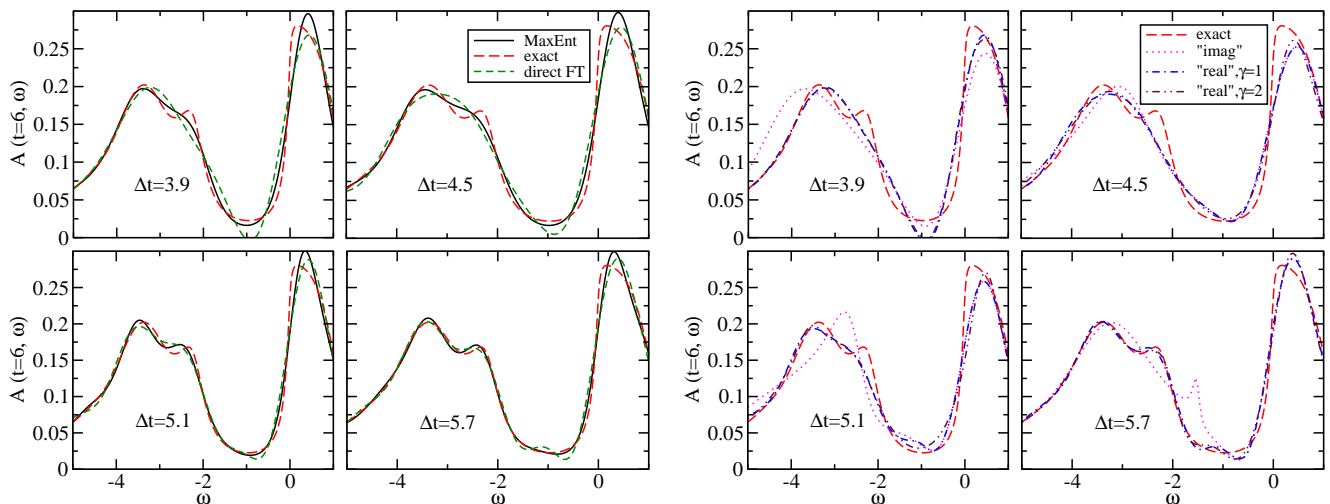


FIG. 12: Convergence of non-equilibrium $A(\omega, t = 6)$ estimates for different short real-time intervals. In the case of the “imag” modified Padé, we set $\beta = 20$ and used 100 data points. For the “real” modified Padé results, we used 100 equidistant data points for $\text{Re } z_n$ on the interval $[-10, 10]$.

the necessary interval length from $\Delta t = 5.7$ to $\Delta t = 4.5$ and thus allows to compute time-dependent spectra up to slightly longer times. Depending on the application, this could save considerable effort, since numerical algorithms typically scale badly (at least as the third power) with the length of the contour. The effect of the modified Padé for z_n on parallel lines to the real axis can to a large extent be interpreted as a smoothening procedure for the direct FT. In particular, the double-peak structure in the direct FT solution at $\Delta t = 5.1$ is strongly suppressed, but still slightly visible. However, the peaks are less pronounced than those of the MEM solution at $\Delta t = 4.5$. The behaviour of the “grid” variant is very similar to the “real” variant, except that the “grid” choice cannot resolve the double-peak structure of the lower band (not shown). When the number of real frequency points is increased, the “grid” result converges to the “real” result. Due to numerical instabilities of the Padé procedure, one is however typically limited to less than 400 grid points.

V. CONCLUSION

We analyzed the usefulness of Keldysh real-time Green’s function data for the computation of equilibrium spectral functions of interacting quantum many-body systems. The ill-posed nature of the inversion corresponding to the determination of the spectral function is reflected in the distribution of singular values of the respective continuation kernel. The conventional Wick rotation of Matsubara data yields an exponentially decaying singular value distribution. We found that including a finite real-time branch to the imaginary-time contour adds a plateau to this distribution, which broadens as the length of the real-time contour is increased. This plateau significantly alleviates the inversion even

for small contour lengths. A further analysis showed that the main gain is more precise high-frequency information of the spectral function. For short contours, the real-time data however provide rather crude results at low frequencies. In order to obtain more accurate estimates of low-energy features such as quasi-particle peaks, it is therefore necessary to include data from the Matsubara branch. With the small frequencies well covered by the Matsubara branch and the high frequencies well covered by a short Keldysh branch, the biggest challenge remains the resolution at intermediate energies.

Our analysis of NCA spectra for the Kondo-lattice model suggests that in order to resolve intermediate energies reasonably well, the length of the real-time contour has to be at least $t_{\text{max}} = 10$ (in units where the bandwidth is 4). In real-time Monte Carlo simulations, it is difficult to reach these times, at least in parameter regimes where low-order perturbation theory is not reliable. It thus appears that the exponential increase in the computational cost with increasing t_{max} in real-time Monte Carlo schemes outweighs the benefits from an alleviated MEM analytical continuation. Nevertheless, the MEM analytical continuation of Keldysh Green functions can be a useful and superior alternative to Padé approximants for semi-analytic methods such as higher order strong-coupling perturbation theory. These methods are very useful in certain parameter regimes, such as elevated temperature, or intermediate to strong interactions. While their implementation on the real-frequency axis is challenging, calculations on the Keldysh contour scale polynomially with t_{max} and the contour-lengths needed for reliable MEM analytical continuation can be reached.

In the calculation of non-equilibrium spectra, it is no longer possible to include the Matsubara branch into the Maximum Entropy procedure. As a consequence, the

resolution of low-energy features of the spectrum worsens dramatically if only short-time data are available. Nevertheless, a comparison to alternative, more straightforward techniques, i.e. direct Laplace transform and the modified Padé approach, showed that the MEM yields slightly more reliable solutions for these spectra. The relevant structures could be established for somewhat shorter time intervals than for the extended Padé approaches.

On a conceptual level, the MEM is superior to the direct Laplace transform and the generalized Padé approach. In practical applications, however, because the advantage of a MEM continuation appears to be rather subtle, it will very much depend on the details of the utilized many-body approach whether an application of

MEM is worth its effort. In any case, the comparison of different approaches can help in deciding which features of a non-equilibrium spectrum are trustworthy.

Acknowledgments

We acknowledge funding from the Deutsche Forschungsgemeinschaft (DFG) via SFB 602, SNF grant PP0022-118866 and FP7/ERC starting grant No. 278023. This work also profited from the GoeGrid initiative and the Gesellschaft für Wissenschaftliche Datenverarbeitung Göttingen (GWDG).

-
- [1] M. Eckstein, M. Kollar and P. Werner, Phys. Rev. Lett. **103**, 056403 (2009).
 - [2] M. Eckstein, M. Kollar and P. Werner, Phys. Rev. B **81**, 115131 (2010).
 - [3] P. Werner, T. Oka, M. Eckstein, and A. J. Millis, Phys. Rev. B **81**, 035108 (2010).
 - [4] A. N. Rubtsov, V. V. Savkin, and A. I. Lichtenstein, Phys. Rev. B **72**, 035122 (2005).
 - [5] P. Werner, A. Comanac, L. de' Medici, M. Troyer, and A. J. Millis, Phys. Rev. Lett. **97**, 076405 (2006).
 - [6] L. Mühlbacher and E. Rabani, Phys. Rev. Lett. **100**, 176403 (2008).
 - [7] P. Werner, T. Oka, and A. J. Millis, Phys. Rev. B **79**, 035320 (2009).
 - [8] N. Tsuji, M. Eckstein and P. Werner, arXiv:1210.0133.
 - [9] M. Eckstein and P. Werner, Phys. Rev. B **82**, 115115 (2010).
 - [10] E. Gull, D. Reichmann and A. J. Millis, Phys. Rev. B **84**, 085134 (2011).
 - [11] M. Eckstein, M. Kollar and P. Werner, Phys. Rev. B **81**, 115131 (2010).
 - [12] M. Eckstein and P. Werner, Phys. Rev. B **84**, 035122.
 - [13] N. Tsuji, T. Oka, H. Aoki and P. Werner, Phys. Rev. B **85**, 155124 (2012).
 - [14] M. Eckstein and M. Kollar, Phys. Rev. B **78**, 245113 (2008).
 - [15] J. K. Freericks, H. R. Krishnamurthy, and Th. Pruschke, Phys. Rev. Lett. **102**, 136401 (2009).
 - [16] J. Schwinger, J. Math. Phys. **2**, 407 (1961)
 - [17] For an introduction into the Keldysh formalism, see, e.g., H. Haug and A.-P. Jauho, *Quantum Kinetics in Transport and Optics of Semiconductors*, Springer, Berlin, 2nd edition, 2008.
 - [18] E. T. Jaynes, Phys. Rev. **106**, 620 (1957)
 - [19] M. Jarrell, J. E. Gubernatis, Physics Reports **269**, 133 (1996).
 - [20] N. Wu, "The Maximum Entropy Method", 162 (1997).
 - [21] R. K. Bryan, Eur. Biophys. J. **18**, 165 (1990).
 - [22] H. Jeffreys, Proceedings of the Royal Society of London, Series A **186**, No. 1007, 453 (1946)
 - [23] M. Jarrell, A. Macridin, K. Mielson, and D.G.S.P. Doluweera, in *Lectures on the Physics of Strongly Correlated Systems XII*, AIP Conference Proc. **1014**, A. Avella and F. Mancini (Eds.), 34 (2008)
 - [24] J. Otsuki, H. Kusunose, P. Werner, and Y. Kuramoto, J. Phys. Soc. Jpn. **76**, 114707 (2007).
 - [25] H. J. Vidberg and J. W. Serene, J. Low Temp. Phys. **29** (1977) 179.
 - [26] P. Werner and M. Eckstein, Phys. Rev. B **86**, 045119 (2012).